Version dated: November 28, 2017

RH: Phasing improves utility of UCEs

# Allele Phasing Greatly Improves the Phylogenetic Utility of Ultraconserved Elements

Tobias Andermann[1,2], Alexandre M. Fernandes[3], Urban Olsson[1,2], Mats Töpel[2,4], Bernard Pfeil[1,2], Bengt Oxelman[1,2], Alexandre Aleixo[5], Brant C. Faircloth[6] and Alexandre Antonelli[1,2,7]

[1]*Department of Biological and Environmental Sciences, University of Gothenburg, SE-41319, Göteborg, Sweden;*

[2]*Gothenburg Global Biodiversity Centre, Box 461, SE-405 30, Göteborg, Sweden*

[3]*Universidade Federal Rural de Pernambuco, Serra Talhada, Brazil*

[4]*Department of Marine Sciences, University of Gothenburg, SE-41319, Göteborg, 41319, Sweden;*

[5]*Museu Paraense Emílio Goeldi, Collection of Birds, Belém, Brazil*

[6]*Department of Biological Sciences and Museum of Natural Science, Louisiana State University, Baton Rouge, LA, U.S.A.*

[7]*Gothenburg Botanical Garden, Göteborg, SE-41319, Sweden*

**Corresponding author:** Tobias Andermann, Department of Biological and Environmental Sciences, University of Gothenburg, Carl Skottsbergs Gata 22B, Göteborg, 41319, Sweden; E-mail: tobias.hofmann@bioenv.gu.se

*Abstract.*— In the era of high-throughput sequencing techniques, it is becoming increasingly easy and affordable to sequence big portions of the genome, also for non-model organisms. But instead of sequencing the complete genome, many phylogenetic studies prefer to focus their sequencing efforts on a selected set of target loci. Sets of target loci are commonly enriched through techniques such as sequence capture. The advantage of this approach is that a higher sequencing depth is reached for these selected loci. Higher sequencing depth does not only lead to more confidence in assembling the target sequences but also reveals the allelic variation within the sequenced individual. Even though this allelic variation constitutes important information of great phylogenetic utility, allele sequences are rarely assembled in phylogenetic studies based on sequence capture data. Instead many scientists use contig sequences, resulting from de novo assembly of sequencing reads, for phylogenetic analyses. Here we show how phased allele sequences can be retrieved from sequence capture data and we demonstrate for the first time a full integration of these allele sequences under the Multispecies Coalescent (MSC) model. We find, based on simulated data, that the common approach of analyzing contig sequences produces biased divergence time estimates, while analyzing allele sequences leads to accurate divergence time estimations. We benchmark our allele phasing workflow with an empirical dataset of Ultraconserved Elements (UCEs), generated from the South American hummingbird genus *Topaza* and demonstrate how UCE allele sequences can be used to infer the genetic structure within a genus that diverged during the last three million years. Our empirical results support the recognition of two species in *Topaza* whose taxonomy has been a matter of recent debate. The results also suggest a high rate of gene flow across large distances of rainforest habitats but rare admixture across the Amazon River. We conclude based on comparisons of different data processing strategies that allele phasing is the most proper processing scheme for UCE data and sequence capture data in general. Therefore we recommend that analyzing allele sequences (and not contig sequences) should

become the "best practice" for sequence capture datasets and thus make available this bioinformatic workflow for future phylogenetic studies.

(Keywords: UCE, SNP, heterozygous sites, Multispecies Coalescent, gene tree, species tree, Mitochondrial Genome, Trochilidae, Birds, Amazon)

Massive Parallel Sequencing (MPS) techniques enable time- and cost-efficient generation of DNA sequence datasets of large fractions or even the entirety of genomes. But instead of sequencing complete genomes, researchers often choose to focus sequencing efforts on a set of target loci in order to achieve higher coverage and thus more reliable sequencing of these target regions (Faircloth et al. 2012, 2013; Mirarab et al. 2014; Smith et al. 2014; Faircloth 2015; Harvey et al. 2016; Meiklejohn et al. 2016). Such multilocus datasets, containing thousands of target loci, are commonly generated through enrichment techniques such as sequence capture (synonym: target enrichment, Gnirke et al. (2009)) prior to sequencing. Sequence capture uses custom designed bait sequences (synonym: probes) that bind to specific genetic regions of interest and which in turn enables specific enrichment of these loci. This ensures that the targeted regions are present in higher copy number and hence will be sequenced at higher coverage by MPS techniques.

Higher sequencing coverage at a given locus reveals important information about allelic variation at that locus, which is particularly interesting for understanding demographic processes such as migration, population sizes and the amount of gene flow between and within populations. For this reason the information lying within allelic variation is commonly applied in population genetic studies, often in form of single nucleotide polymorphisms (SNPs). However, it is rarely acknowledged that allelic sequences harbor huge potential for phylogenetic studies as well, in particular concerning the estimation of gene trees and species trees (Potts et al. 2014), and the estimation of divergence times (Lischer et al. 2014). Further, ignoring allelic variation can introduce biases in downstream analyses (Lischer et al. 2014; Garrick et al. 2010).

Despite their excellent utility, allele sequence data are rarely compiled for phylogenetic studies based on MPS data, with only few exceptions (Lischer et al. 2014; Potts et al. 2014; Schrempf et al. 2016). This is surprising since most MPS generated datasets, in particular those resulting from sequence capture enrichment, are very suitable

for compiling allelic sequences for any given locus in the dataset. Instead most phylogenetic studies generate and analyze contig sequences for each locus, thereby masking the allelic information that lies within the MPS data (see Results, Fig. 4). Part of the reason for the common neglection of such useful information is that the computational tools that help with the compilation of allelic information require bioinformatic knowledge that exceeds the experience of the average biologist working with MPS sequence data. Up to this point and to the authors best knowledge, none of the MPS processing pipelines contained user friendly solutions for the compilation of allele sequences. We therefore integrated an allele phasing function in the open-source PHYLUCE pipeline (Faircloth 2015).

Additionally to challenges with compiling allelic sequences, also the proper analysis of allelic information in phylogenetic studies remains challenging and is an intensively discussed topic (Garrick et al. 2010; Lischer et al. 2014; Potts et al. 2014; Schrempf et al. 2016). Various researchers have chosen different approaches to include this information into phylogenetic methods. One such approach has been to code heterozygous sites using IUPAC ambiguity codes and to include these as additional characters into existing substitution models for gene tree and species tree inference (Potts et al. 2014; Schrempf et al. 2016). While these studies demonstrated that integrating this additional information leads to a higher accuracy in phylogenetic inference, Lischer et al. (2014) found that coding heterozygous sites as IUPAC ambiguity codes in phylogenetic models biases the results toward older divergence time estimates. Instead Lischer et al. (2014) introduce their method of repeated random haplotype sampling (RRHS) in which they repeatedly concatenate AFLP sequences (Amplified fragment length polymorphisms), choosing a random haplotype for any given locus in each concatenation replicate. In their approach they then analyze thousands of concatenation replicates separately for phylogenetic tree estimation and summarize the results between replicates, thereby integrating the allelic information in form of uncertainty intervals. However there are two important shortcomings

of the approach presented by Lischer et al. (2014): 1. concatenating unlinked loci and in particular allele sequences from unlinked loci in a random manner is known to produce incorrect topologies (Degnan and Rosenberg 2009) often with false confidence (Edwards et al. 2007; Kolaczkowski and Thornton 2004; Kubatko and Degnan 2007; Mossel and Vigoda 2005), which is not accounted for when doing so repeatedly and summarizing the resulting trees and 2. running thousands of tree estimation replicates based on extensive amounts of sequence data does result in unfeasibly long computation times, particularly for Markov-Chain Monte Carlo (MCMC) based softwares such as MrBayes or BEAST.

Here we introduce the bioinformatic assembly of allele sequences for UCE data and demonstrate a full integration of these sequences under the Multispecies Coalescent (MSC) model for both empirical and simulated data. In our approach we treat each allelic sequence of an individual at a given locus as an independent sample from the population. We analyze these sequences using the species tree and delimitation software STACEY (Jones et al. 2014; Jones 2017), which does not require a priori clade- or species-assignments and therefore allows us to effectively treat each allele sequence as an individual sample. We demonstrate the utility of our approach by resolving the shallow genetic structure (<1 Ma) within the two recognized morphospecies of the South American hummingbird genus *Topaza*. The underlying sequence data of 2,386 Ultraconserved Elements (UCEs, see Faircloth et al. (2012)) was generated through sequence capture using the bait set for Tetrapods (see `http://ultraconserved.org`) and subsequent Illumina sequencing. We find, based on simulations, that allele sequences yield more accurate results in terms of species tree estimation and species delimitation than the classic contig sequence approach, which ignores heterozygous information. Our simulation results further show that proper phasing of allele sequences outperforms alternative approaches of coding heterozygous information, such as sequences containing IUPAC ambiguity codes or Single Nucleotide Polymorphisms (SNPs). We conclude that phasing sequence capture data can

be critical for correct species delimitation and phylogeny estimation, particularly in recently diverged groups, and that analyses using phased alleles should therefore become the preferred choice for sequence capture datasets.

# Materials and Methods

## *Study System*

The genus *Topaza* together with its sister genus *Florisuga* form the Topazes group, which together with the Hermits represent the most ancient branch within the hummingbird family (Trochilidae) (McGuire et al. 2014). Topazes are estimated to have diverged as a separate lineage from all other hummingbirds around 21.5 Ma, whereas the most recent common ancestor (MRCA) of *Topaza* and *Florisuga* lived approximately 19 Ma (McGuire et al. 2014). At present there are two morphospecies recognized within *Topaza*, namely the Fiery Topaz *T. pyra* (Gould, 1846) and the Crimson Topaz *T. pella* (Linnaeus, 1758). However, the species status of *T. pyra* has been challenged by some authors (Schuchmann 1999; Ornés-Schmitz and Schuchmann 2011), who consider this genus to be monotypic. Topaz hummingbirds are endemic to the Amazonian rainforest and are some of the most spectacular and largest hummingbirds worldwide, measuring up to 23 cm (adult males, including tail feathers) and weighing up to 12 g (Schuchmann et al. 2016; del Hoyo et al. 2016a). These birds are usually found in the forest canopy along forest edges and clearings, and they are often seen close to river banks (Ornés-Schmitz and Schuchmann 2011). There is morphological evidence for several subspecies within both currently recognized *Topaza* species (Peters 1945; Schuchmann 1999; Hu et al. 2000; Ornés-Schmitz and Schuchmann 2011) that we investigate using genetic data.

## *Sequence Data Generation*

We extracted DNA from 10 vouchered hummingbirds (9 *Topaza*, one *Florisuga*, see Table 1) from muscle tissue using the Qiagen DNeasy Blood and Tissue Kit according to the manufacturer's instructions (Qiagen GmbH, Hilden, Germany). These samples cover most of the genus' total geographic range (Fig. 1) and all morphologically recognized intraspecific taxa (Schuchmann et al. 2016; del Hoyo et al. 2016a). All samples were sonicated with a Covaris S220 sonication device in order to break the genomic DNA into shorter fragments with a targeted fragment length of 800 bp. Paired-end, size-selected DNA libraries were prepared for sequencing on the Illumina MiSeq platform, using the magnetic-bead based NEXTflexTM Rapid DNA-Seq Kit (Bioo Scientific Corporation, Austin, TX, USA), following the user's manual (v14.02).

We used the "Tetrapods-UCE-2.5Kv1" bait set (`uce-2.5k-probes.fasta`), consisting of 2,560 baits (each 120 bp), targeting 2,386 UCEs, as described by Faircloth et al. (2012). The bait sequences were downloaded from `http://ultraconserved.org` and synthesized by MYcroarray (Biodiscovery LLC, Ann Arbor, MI, USA). Sequence enrichment was performed using a MYbaits kit according to the enclosed user manual (v1.3.8). The enriched libraries were then sequenced using 250 bp, paired-end sequencing on an Illumina MiSeq machine (Illumina Inc., San Diego, CA, USA). Library preparation, sequence enrichment and sequencing were performed by Sahlgrenska Genomics Core Facility in Gothenburg, Sweden.

## *Mitochondrial Genome*

Even though no baits targeting mitochondrial loci were used during sequence capture, we found that as many as 4.5% of all sequence reads were of mitochondrial origin. This was sufficient to assemble the complete mitochondrial genome for all samples, which

Table 1: Information of the specimens sequenced. Subspecies identifications based on morphological characters, which are hard to distinguish in this group. Abbreviation for sample providers: INPA = Instituto Nacional de Pesquisas da Amazônia, MPEG = Museum Paraense Emílio Goeldi, USNM = NMNH, Smithsonian Institution, Washington DC, USA.

| **ID** | **Taxon** | **Subspecies** | **Voucher number** | **Latitude** | **Longitude** |
|---|---|---|---|---|---|
| 1 | *Topaza pyra* | *amaruni* | INPA A1106 | -0.044167 | -66.94944 |
| 2 | *T. pyra* | *pyra* | MPEG 62475 | -1.559444 | -65.88006 |
| 3 | *T. pyra* | *pyra* | MPEG 62474 | -4.083889 | -60.66050 |
| 4 | *T. pyra* | *pyra* | MPEG 52721 | -7.350000 | -73.66667 |
| 5 | *T. pella* | NA | USNM 586322 | 7.220000 | -60.29000 |
| 6 | *T. pella* | *pella* | INPA A3319 | -1.927900 | -59.41600 |
| 7 | *T. pella* | *smaragdula* | MPEG 61688 | -1.950000 | -51.60000 |
| 8 | *T. pella* | *microrhyncha* | MPEG 65603 | -5.352417 | -57.47500 |
| 9 | *T. pella* | NA | INPA A6233 | -9.028550 | -64.24231 |
| 10 | *Florisuga fusca* | NA | MPEG 70697 | -15.15972 | -39.04500 |

we analyzed in BEAST (Drummond et al. 2012) in order to infer a dated mitochondrial genealogy. Dating priors included clock-rate priors for three mitochondrial genes, estimated for honeycreepers by Lerner et al. (2011) and node-age priors within the genus *Topaza* that were estimated by McGuire et al. (2014). A detailed description of the assembly and analysis of the mitochondrial genome data can be found in online Appendix 1 (Supplemental Material available on Dryad).

## *UCE Data Processing*

For this study we generated five different types of datasets, which we analyzed under the MSC. These five datasets, representing different coding schemes of heterozygous information, are listed and described in the following.

*1. UCE contig alignments.*— In this study we use the term contig in a simplified manner to refer to the consensus sequence derived from the actual contig (de novo assembly of overlapping sequence reads). Many de novo assemblers generate these contig consensus

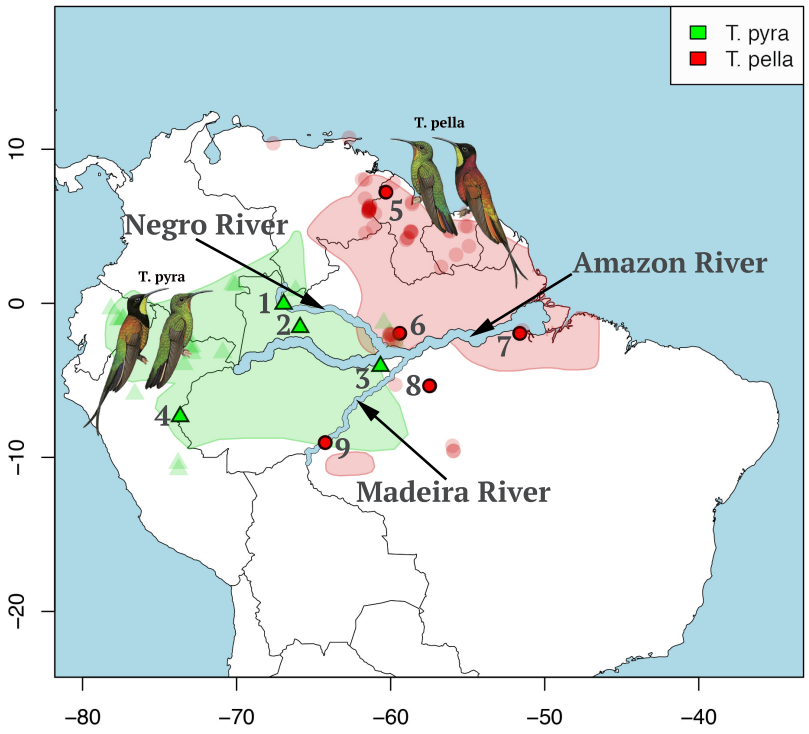


Figure 1: Map of northern South America, showing sampling locations (numbered symbols) of *Topaza* specimens. Numbers represent sample IDs (Table 1). The colored polygons show the distribution range of the two morphospecies (*T. pyra* = green, *T. pella* = red) as estimated by BirdLife International (`http://www.birdlife.org`). Transparent symbols (triangles and circles) represent *Topaza* sightings, which were downloaded from the eBird database (Sullivan et al. 2009). The major river systems in the Amazon drainage basin are marked in blue (not in proportion). *Topaza* illustrations were provided by del Hoyo et al. (2016b).

sequences by ignoring variants at heterozygous positions and instead treat them like sequencing errors by choosing the more probable variant, while discarding the other (Iqbal et al. 2012). Since contig sequences generated in this manner are commonly used in phylogenetic analyses of MPS datasets (e.g. Faircloth et al. (2012); Smith et al. (2014); Faircloth (2015)), we generated contig MSAs for all UCE loci in order to test the accuracy of the phylogenetic estimation of this approach.

To create multiple sequence alignments (MSAs) from UCE contig data, we followed the suggested workflow from the PHYLUCE documentation

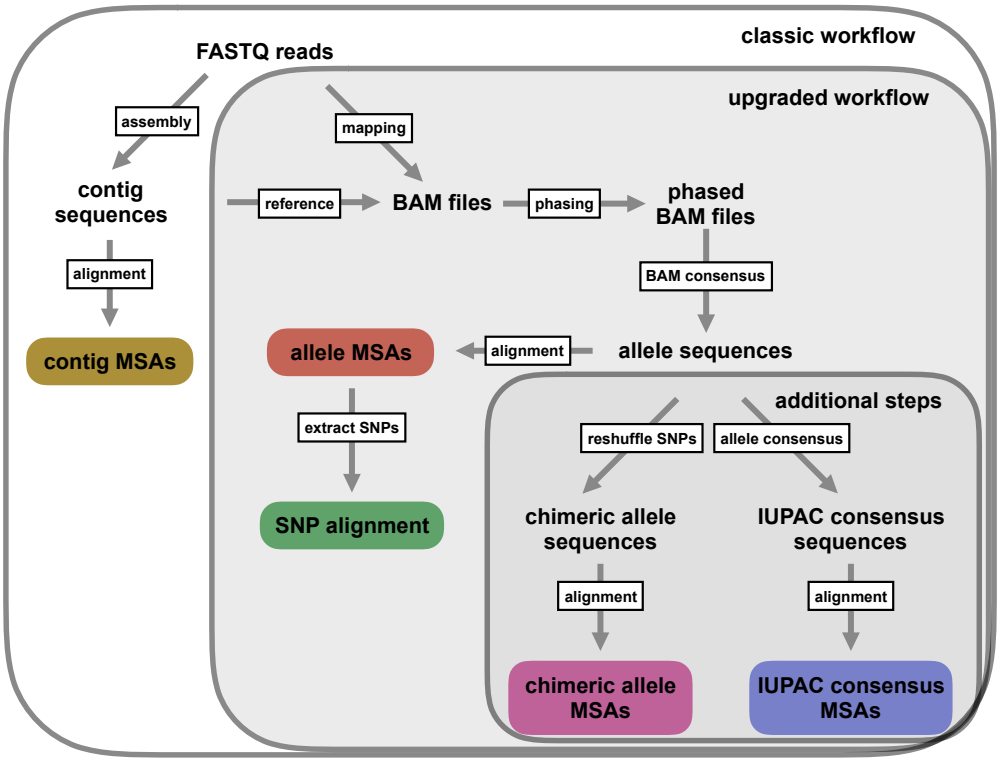


Figure 2: Depiction of the workflow developed here. Colored boxes represent different types of multiple sequence alignments (MSAs) used for phylogenetic inference in this study. In addition to the standard UCE workflow of generating contig MSAs (Faircloth et al. 2012; Smith et al. 2014; Faircloth 2015), we extended the bioinformatic processing in order to generate UCE allele MSAs, and to extract SNPs from these allele MSAs. We added these new functions to the PHYLUCE pipeline (Faircloth 2015). Additional steps of data processing were executed in this study in order to test different codings of heterozygous positions.

(`http://phyluce.readthedocs.io/en/latest/`). We applied the PHYLUCE default settings unless otherwise stated. First we quality-filtered and and cleaned raw Illumina reads of adapter contamination with Trimmomatic (Bolger et al. 2014), which is implemented in the PHYLUCE function `illumiprocessor`. The reads were then assembled into contigs using the software ABYSS (Simpson et al. 2009) as implemented in the PHYLUCE pipeline. In order to identify contigs representing UCE loci, all assembled contigs were mapped against the UCE reference sequences from the bait sequence file

(`uce-2.5k-probes.fasta`), using the PHYLUCE function `match_contigs_to_probes.py`. We extracted only those sequences that matched UCE loci and that were present in all samples (n=820). These UCE sequences were then aligned for each locus (Fig. 2) using MAFFT (Katoh et al. 2009).

*2. UCE allele alignments.*— We altered the typical UCE workflow in order to retrieve the allelic information that is lost when collapsing multiple reads into a single contig sequence (Fig. 2). To create this new workflow, we extracted all UCE contigs for each sample separately and treated each resulting contig set as a sample-specific reference library for read mapping. We then mapped the cleaned reads against each reference library on a per sample basis, using CLC-mapper from the CLC Workbench software. The mapped reads were sorted and then phased with SAMtools v0.1.19 (Li et al. 2009), using the commands `samtools sort` and `samtools phase`, respectively. This phasing function is based on a dynamic programming algorithm that uses read connectivity across multiple variable sites to determine the two phases of any given diploid locus (He et al. 2010). Further, this algorithm uses paired-end read information to reach connectivity over longer distances and it minimizes the problem of accidentally phasing a sequencing error, by applying the minimum error correction function (He et al. 2010).

UCE data provide an excellent dataset for allele phasing based on read connectivity, since the read coverage across any given UCE locus typically is highest in the center and decreases toward the ends, which makes it possible to phase throughout the complete locus without any breaks in the sequence. Even in cases where the only variable sites are found on opposite ends of the locus, the fragment length we selected for in this study (800 bp) in combination with paired-end sequencing, enables the phasing process to bridge across the complete locus. The two phased output files (BAM format) were inspected for proper variant separation for all loci using Tablet (Milne et al. 2013). We then collapsed each

BAM file into a single sequence and exported the two resulting allele sequences for each sample in FASTA format. In the next step we aligned the allele sequences between all samples, separately for each UCE locus, using MAFFT (Fig. 2). We integrated this complete workflow into the UCE processing software PHYLUCE (Faircloth 2015) with slight alterations, one of which is the use of the open-source mapping program bwa (Li and Durbin 2010) in place of CLC-mapper.

*3. UCE IUPAC consensus sequence alignments.*— We generated an additional set of alignments by merging the two allele sequences for each individual into one consensus sequence with heterozygous sites coded as IUPAC ambiguity codes. We used this dataset in order to test if our allele phasing approach leads to an improved phylogenetic inference in comparison to the IUPAC consensus approach as applied in other studies, in which heterozygous positions are coded as IUPAC ambiguity codes in a consensus sequence for each locus and individual (Potts et al. 2014; Schrempf et al. 2016).

*4. UCE chimeric allele alignments.*— In this study we also investigate whether correct phasing of heterozygous sites is essential or if equal results are achieved by randomly placing variants on either one allele sequence. For this purpose we generated another dataset with chimeric allele sequence alignments. These alignments were generated by applying a custom python script to the phased allele sequence alignments, which randomly shuffles the two variants at each polymorphic position between the two allele sequences for each individual. This process leads in many cases to an incorrect combination of variants on each allele sequence, thereby creating chimeric allele sequences. The resulting alignments contain the same number of sequences as the phased allele alignments (two sequences per individual), while the contig alignments and the IUPAC consensus alignments contain only half as many sequences (one sequence per individual).

*5. UCE SNP alignment.*— A common approach of analyzing heterozygous information is to reduce the sequence information to only a single variant SNP per locus. This data-reduction approach is often chosen because multi locus datasets of the size generated in this study can be incompatible for full sequence based phylogeny estimation with Bayesian MSC methods, due to unfeasibly long computational times. Instead of full sequence alignments, alignments of unlinked SNPs can be used to infer species trees and species demographics under the MSC model with the BEAST2 package SNAPP (Bryant et al. 2012), a program specifically designed for such data. However, extracting and filtering SNPs from BAM files with existing software (such as the Genome Analysis Toolkit (GATK), McKenna et al. (2010)) and converting these into a SNAPP compatible format can be cumbersome, as SNAPP requires positions with exactly two different states, coded in the following manner: individual homozygous for the original state = "0", heterozygous = "1", and homozygous for the derived state = "2".

We therefore developed a python function, which extracts biallelic SNPs directly from allele sequence MSAs. Extracting SNPs from MSAs in this manner is a straightforward and simple way to generate a SNP dataset compatible with SNAPP, and does not require re-visiting the BAM files. Our SNP extraction script outputs a SNP alignment file that is formatted for input in SNAPP. We applied this function to the phased UCE alignments and extracted one position per alignment (to ensure unlinked SNPs) that had exactly two different states among all *Topaza* samples, not allowing for positions with missing data or ambiguities. This resulted in a SNP dataset of 598 unlinked loci. We integrated the SNP extraction from allele sequence MSAs into the PHYLUCE pipeline.

## *Generation of Simulated UCE Data*

In order to assess the accuracy of the phylogenetic inferences resulting from different data processing approaches, we generated simulated UCE data for all five processing schemes as

applied to the empirical *Topaza* data. For each of the five processing schemes we generated and analyzed ten independent simulation replicates.

*1. Simulated allele alignments.*— We estimated parameters of species divergence times and population sizes under the MSC model (Rannala and Yang 2003) from the empirical UCE allele alignments using the Bayesian MCMC program BPP v3.1 (Yang 2015). We applied the A00 model implemented in the software, which estimates divergence times and population sizes when the species tree topology is provided. As input, we chose the species tree topology that resulted from the analysis of the allele sequence data in STACEY, assigning the *Topaza* samples to five separate taxa (corresponding to colored clades in Fig. 6b). An initial BPP analysis did not converge in reasonable computational time, a problem that has been reported before for UCE datasets of several hundred loci (Giarla and Esselstyn 2015). We therefore split the 820 UCE alignments randomly into 10 subsets of equal size (n=82) and analyzed these separately with identical settings in BPP. The MCMC was set for 150,000 generations (burn-in 50,000), sampling every 10 generations. We summarized the estimates for population sizes and divergence times between all 10 individual runs. We then applied the mean values of these estimates to the species tree topology, by using the estimated divergence times as branch lengths and estimated population sizes as node values, resulting in the species tree in Fig. 6g. This tree was used to simulate sequence alignments with the MCcoal simulator, which is integrated into BPP. Equivalent to the empirical data, we simulated sequence data for five taxa (D, E, X, Y, and Z) and one outgroup taxon (F, not shown in Fig. 6g). In the simulations these taxa were simulated as true species under the MSC model. In order to mimic the empirical allele data, we simulated four individuals for species 'D' (equivalent to two allele sequences for 2 samples), four for species 'E', four for species 'X', two for species 'Y' (two allele sequences for one sample), four for species 'Z', and two for the outgroup species 'F'. In this manner

we simulated 820 UCE allele MSAs of 848 bp length (= average alignment length of empirical allele alignments).

*2. Simulated contig alignments.*— In order to simulated UCE contig MSAs, we merged the sequences within each coalescent species in pairs of two (equivalent to pairs of allele sequences). Each pair of sequences was joined into one sequence by randomly picking one of the two variants in the case of a polymorphism (heterozygous site). This we used to represent the UCE contig approach of previous studies (Faircloth et al. 2012; McCormack et al. 2012; Smith et al. 2014; Faircloth 2015) that rely on UCE contig data as generated by assemblers such as ABYSS, Velvet or Trinity, which pick only one of the two variants at a heterozygous site. Just as in the empirical assembler approach, our simulation approach may generate chimeric contig sequences.

*3. Simulated IUPAC consensus alignments.*— Next, we generated IUPAC consensus MSAs in the same manner as we generated the simulated contig MSAs in the previous step, with the exception that heterozygous sites were coded with IUPAC ambiguity codes (instead of randomly picking one of the two variants).

*4. Simulated chimeric allele alignments.*— We generated chimeric allele sequence MSAs from the simulated allele MSAs, by randomly shuffling the heterozygous sites between each pair of sequences (same pairs as in the previous two steps).

*5. Simulated SNP alignment.*— Finally, we extracted two different SNP datasets from the simulated phased allele MSAs. The first SNP dataset (SNPs complete) was extracted in the same manner as described above for the empirical data (one SNP per locus) which resulted in a total alignment length of 820 SNPs for the simulated data. We extracted an additional SNP dataset (SNPs reduced) from only the subset of the 150 simulated allele alignments that were used for the sequence-based MSC analyses (see next section below).

The resulting SNP dataset of 150 SNPs was used to compare the phylogenetic inference resulting from SNP data versus that resulting from full sequence data, if the same number of loci is being analyzed.

## *MSC Analyses of Empirical and Simulated UCE Data*

*Sequence-based tree estimation.*— In order to jointly infer gene trees and species trees, we analyzed each of the generated sets of MSAs (processing schemes 1-4 for empirical and simulated) under the MSC model, using the DISSECT method (Jones et al. 2014) implemented in STACEY (Jones 2017). STACEY is available as a BEAST2 (Bouckaert et al. 2014) package. STACEY allows *BEAST analyses without prior taxonomic assignments, searching the tree space while simultaneously collapsing very shallow clades in the species tree (controlled by the parameter collapseHeight). This collapsing avoids a common violation of the MSC model that occurs when samples belonging to the same coalescent species are assigned to separate taxa in *BEAST. This feature makes STACEY very suitable for analyzing allele sequences, as they don't have to be constrained to belonging to the same taxon and hence can be treated as independent samples from a population. STACEY runs with the usual *BEAST operators, but integrates out the population size parameter and has more efficient species tree change operators that decrease the time until convergence significantly. In order to reach even faster convergence, we reduced the number of loci for this analysis by selecting the 150 allele MSAs with the most parsimony informative sites. This selection was made for both the empirical and the simulated allele MSAs. The same loci were selected for all other processing schemes.

We estimated the most appropriate substitution model for each of the 150 loci with jModeltest (Supplementary Table S1 available on Dryad). We then applied the resulting best substitution model for each locus selected by the BIC to the alignments in BEAUTI

v2.4.4. We did not apply any taxon assignments, thereby treating every sequence as a separate taxon. We chose a strict clock and the STACEY-specific BirthDeathCollapse model as species tree prior, choosing a value of 1e-5 for the collapseHeight parameter. Other settings were: bdcGrowthRate = log normal (M=4.6, S=1.5); collapseWeight = beta (alpha=2, beta=2); popPriorScale = log normal (M=-7, S=2); relativeDeathRate = beta (alpha=1.0, beta=1.0). Additionally we set the clock rate for each locus to a log normal distribution with M=0 and S=1. For the IUPAC consensus data, we enabled the processing of ambiguous sites by adding `useAmbiguities="true"` to the gene tree likelihood priors for all loci in the STACEY XML file. All analyses were run for 1,000,000,000 MCMC generations or until convergence (ESS values >200), logging every 20,000 generations. Convergence was assessed using Tracer v1.6 (Rambaut et al. 2013). We then summarized the posterior tree distribution into one maximum clade credibility tree with TreeAnnotator v2.4.4 discarding the first 10% of trees as burn-in. For the simulated data, the posterior species tree distributions of each analysis were analyzed with the program SpeciesDelimitationAnalyser (part of the STACEY distribution). This program produces a similarity matrix that contains the posterior probabilities of belonging to the same cluster for each pair of sequences. This analysis was run with a collapseHeight value of 1e-5 (identical to the collapseHeight used in the STACEY analysis), while discarding the first 10% of trees as burn-in.

*SNP-based tree estimation.*— In order to estimate the species tree phylogeny from the extracted SNP data, we analyzed the empirical and simulated SNP data in SNAPP. We did not apply any prior clade assignments to the samples in the SNP alignment (each sample was assigned as its own taxon). Coalescent rate and mutation rates were set to be estimated based on the input data. We chose a Yule species tree model with default settings ($\lambda = 0.00765$). We ran the analysis for 10,000,000 generations, sampling trees and

other parameters from the posterior every 1,000 generations. Differently to STACEY, SNAPP assumes correct assignments of all sequences to coalescent species. Using the simulated SNP data we therefore tested how our approach of assigning every individual as its own coalescent species affects the resulting phylogenetic inference. We did so by running a separate analysis for both simulated SNP datasets (complete and reduced) with correct species assignments (assignments as in Fig. 6g).

# Results

## *Mitochondrial Tree (BEAST)*

The BEAST analysis of the complete mitochondrial genomes (see online Appendix 1) produced a fully resolved gene tree topology (Fig. 3). All nodes are supported by 100% Bayesian posterior probability (PP). The divergence between the two lineages *T. pyra* and *T. pella* is inferred at 2.36 Ma, with 95% of the highest posterior density (HPD) ranging between 1.96 and 2.78 Ma. The tree also shows a separation of two distinct lineages within *T. pyra* inferred at 0.68 Ma (95% HPD: 0.54 - 0.84 Ma), dividing the samples of this morphospecies into a northern and a southern clade, separated by the Amazon River (Fig. 1). A similar, yet slightly more recent split can be seen within *T. pella*. This split of lineages is estimated to 0.39 Ma (95% HPD: 0.30 - 0.48 Ma), revealing the same pattern of one northern and one southern clade with the exception of sample 7; this sample from the southern bank of the Amazon River delta is placed together with the samples derived from localities north of the Amazon (samples 5 and 6) in the mitochondrial tree. Below, we refer to those individuals sampled north of the Amazon River as "northern" and to those sampled south of the Amazon as "southern".

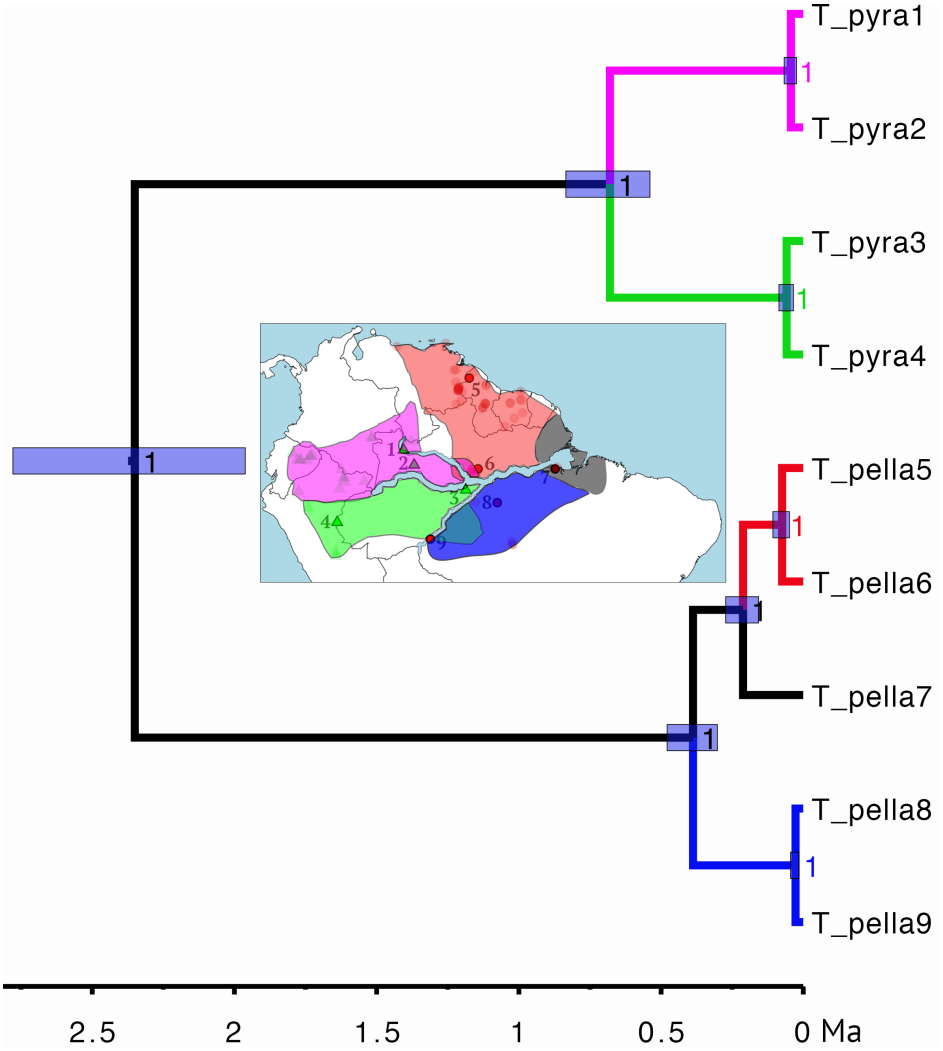


Figure 3: Mitochondrial phylogeny estimated from complete mitochondrial genomes in BEAST. Node support values represent PP. The blue bars at nodes represent the 95% HPD of divergence times. Scale axis shows time units in millions of years. The map in the center shows the potential ranges of the clades that are found in the mitochondrial tree (color-coded). The ranges are based on the BirdLife distribution ranges (Fig. 1) and have been expanded in order to accommodate all *Topaza* occurrence data.

## *UCE Summary Statistics*

*Alignment statistics.*— In the following we use the term polymorphic sites for those positions within a MSA alignment of a given locus, for which we find at least two different states among the sequences for all samples. This does not require any of the samples being

heterozygous for the given position, since we do not search for SNPs on a per sample basis but rather for SNPs within the genus *Topaza* (for the following statistics we are excluding the outgroup). In this manner we find that the empirical UCE contig alignments have an average of 2.8 polymorphic sites per locus (average alignment length = 870 bp). In contrast, phasing the empirical UCE data leads to 4.5 polymorphic sites per locus and an average alignment length of 848 bp for the UCE allele alignments, representing a 60% increase in polymorphic sites per locus. This increase of polymorphic sites is attributable to the fact that many variants get lost during contig assembly, since ABYSS (and other tested contig assemblers, namely Trinity and Velvet) eliminate one of the two variants at a heterozygous locus. The reduced alignment length of the allele alignments in comparison to the contig alignments is due to conservative alignment clipping thresholds, which lead to a clipping of the alignment ends, if less than 50% of sequences are present. Since the allele phasing algorithm divides the FASTQ reads into two allele bins and since a nucleotide is only called if it is supported by at least three high-quality FASTQ reads, we loose some of the nucleotide calls at areas of low read coverage (mostly at the ends of a locus) in the allele sequences in comparison to the contig sequences. Hence the alignment clipping mechanism reduces the alignment length of allele sequence MSAs in average more than for contig sequence MSA.

More information about the distribution of lengths and variable sites within the empirical UCE data can be found in the Supplementary Figs. S1 and S2 available on Dryad. The simulated contig MSAs have an average of 3.2 polymorphic sites per locus, after excluding the outgroup, resulting to a clade, which is the equivalent to the *Topaza* clade in the empirical data. The simulated allele MSAs, on the other hand, contain an average of 5.4 polymorphic sites (69% increase). An overview of parsimony informative sites, variable sites and length of each alignment (simulated and empirical data) can be found in Supplementary Table S2 available on Dryad.

*ABYSS does not detect heterozygous sites.*— Since ABYSS occasionally produces sequences containing IUPAC ambiguity codes, possibly representing heterozygous sites, we checked exemplary for one sample (sample 5, *T. pella*) whether we find the same sites to be heterozygous in the phased allele sequences. The results are striking, since not a single heterozygous site within sample 5 that was detected in our allele sequence was coded as a IUPAC ambiguity code in the ABYSS contigs (e.g. Fig 4a). While our phasing approach revealed 343 heterozygous UCE loci with a total of 728 SNPs in sample 5, only 26 UCE loci contained IUPAC ambiguity codes (degenerate bases) in the contigs resulting from the ABYSS de novo assembly. For all other loci, ABYSS assumes complete homozygosity, as the resulting contig sequences are free of ambiguity codes. Within the 26 loci with IUPAC ambiguity codes, ABYSS introduced 473 degenerate bases, most of which constitute blocks of N's. Effectively all of these ambiguous positions are in places of extremely low FASTQ read coverage (<2 reads per haplotype), with the exception of 6 positions that are covered by >2 reads per haplotype. However, even those 6 positions don't represent true heterozygous sites within sample 5, which becomes apparent when looking at the phased allele sequences or the FASTQ reads at those loci (e.g. Fig. 4b).

## *MSC Results of Empirical UCE Data*

The MSC species tree results for all tested processing schemes of the empirical UCE data (contig sequences, allele sequences, IUPAC consensus sequences, chimeric allele sequences and SNPs) converge on a similar species tree topology, yet with no consistent topology being inferred within *T. pyra* (Fig. 5 and Supplementary Fig. S3 available on Dryad). All analyses strongly support the monophyly of both *T. pyra* and *T. pella* with 100% PP. In all MSC analyses we also see strongly supported genetic structure within *T. pella* ($\geq$ 97% PP), separating the northern samples (5 and 6) from the southern ones (7, 8 and 9). Additionally, within the shallow southern *T. pella* clade, all datasets, with exception of the

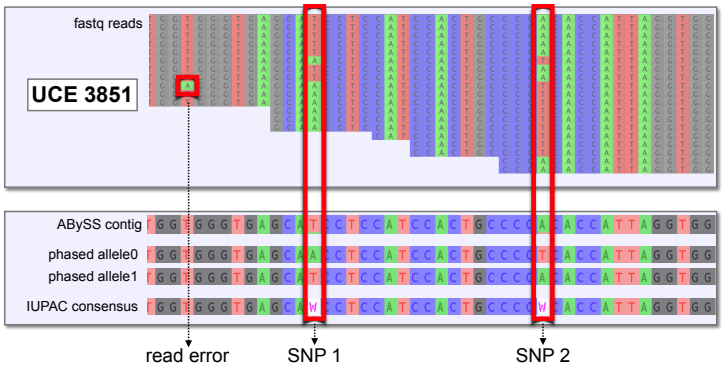


(a) Heterozygous position picked up by allele phasing

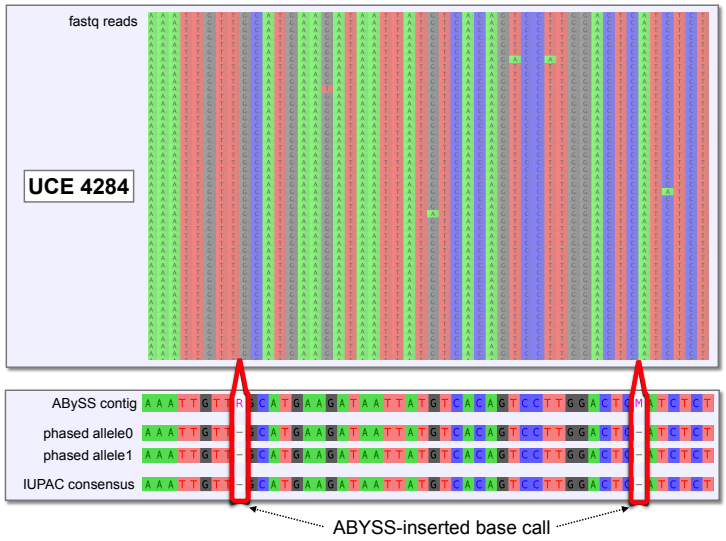


(b) Erroneous insertion of IUPAC ambiguity by ABYSS

Figure 4: Detection of heterozygous sites in FASTQ reads. The figure shows two UCE loci for sample 5 (*T. pella*). Displayed in both cases are the FASTQ reads, the ABYSS contig sequence, the two phased allele sequences and the correct IUPAC consensus sequence generated from our phased allele sequences. (a) An example of true heterozygous sites, which are correctly represented in the phased allele sequences sequences but not coded as IUPAC ambiguity in the ABYSS contig. Instead ABYSS makes a majority call for this position, thereby masking the heterozygous site by eliminating one of the two variants. This is the case for all heterozygous sites that were picked up by the allele sequences in our data. (b) An example of a UCE locus that carries IUPAC ambiguity codes in the ABYSS contig sequence, as was the case for 26 UCE loci in our data. The ambiguity calls at these positions are not supported by the FASTQ reads but are inserted by ABYSS at random positions and are thus not correct. Our phased allele sequences on the other hand represent the FASTQ reads correctly and do not call this position as heterozygous. This was the case for all 26 loci in our data with ABYSS-inserted IUPAC ambiguity codes.

IUPAC consensus data (Fig. 5c), strongly support a genetic distinction ($\geq$ 99% PP) between sample 7 from the Amazon River delta and the other southern *T. pella* samples (8 and 9). The deep split between northern and southern samples within *T. pyra* on the other hand, which we find in the mitochondrial tree (Fig. 3), is not very well supported by the multilocus MSC analyses. However, the analysis of the allele dataset returns a phylogenetic signal, possibly tracking a genetic divergence between these two clades, but their monophyly is not very strongly supported (Fig. 5b).

## *MSC Results of Simulated Data*

*Species tree topology.*— For the simulated data we analyzed six different datasets under the MSC model: contig sequence MSAs (n=150, STACEY), allele sequence MSAs (n=150, STACEY), IUPAC consensus MSAs (n=150, STACEY), chimeric allele MSAs (n=150, STACEY), reduced SNP data (n=150, SNAPP), and the complete SNP dataset (n=820, SNAPP). All resulting species trees (Figs. 6a to 6f) correctly return the topology of the species tree that was used to simulate the data (Fig. 6g). All central nodes in the species trees are supported by $\geq$90% PP in all analyses, with the exception of the species tree resulting from the reduced SNP dataset, which shows very weak support for two nodes and has a large uncertainty interval around the root-height (Fig. 6e). However, these shortcomings disappear when adding more (unlinked) SNPs to the dataset (Fig. 6f). The full SNP dataset (n=820) produces the correct species tree topology with high node support consistently throughout ten independently simulated datasets (Supplementary Fig. S4 available on Dryad). The SNAPP species tree topology appears in our case to be unaffected by the chosen clade assignments model; while we allowed every sequence to be it's own taxon in Figs. 6e and 6f we ran additional analyses in which we applied the correct species assignment (Fig. 6g) to both SNP datasets (reduced and complete SNP data),

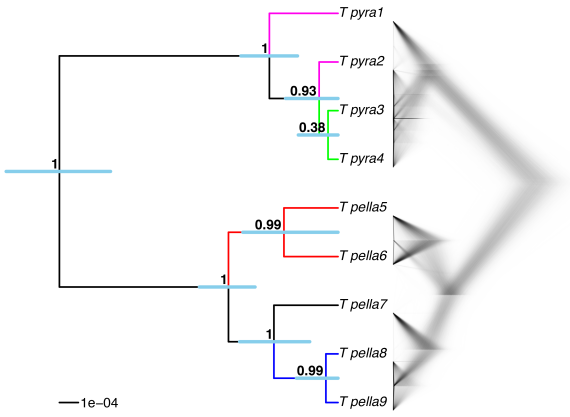


(a) Contig sequence alignments (n=150)

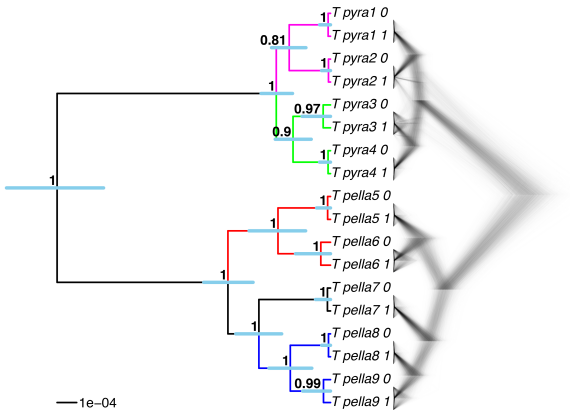


(b) Phased allele alignments (n=150)

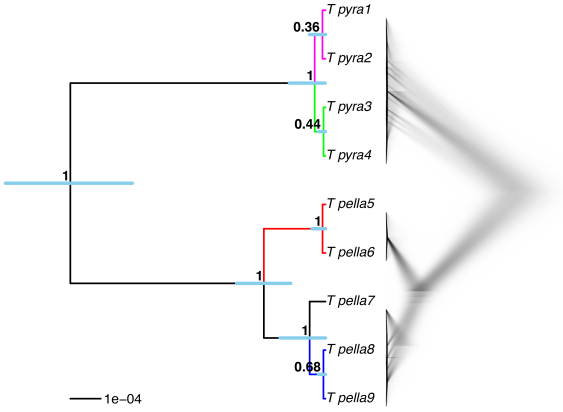


(c) IUPAC consensus alignments (n=150)

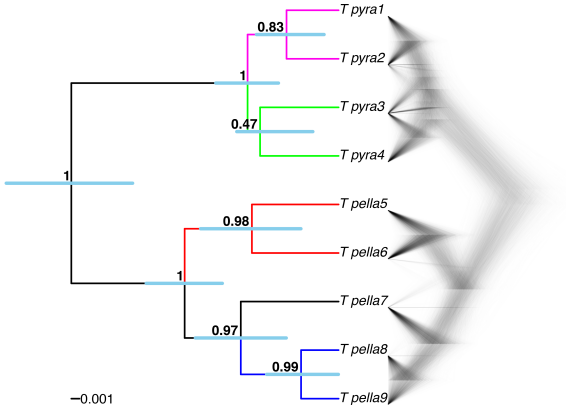


(d) SNPs (n=598)

Figure 5: MSC species trees for the empirical *Topaza* data, based on four different data types used in this study: contig sequence MSAs, phased allele sequence MSAs, IUPAC consensus sequence MSAs and SNP data. (a) STACEY species tree from UCE contig alignments (n=150), (b) STACEY species tree from UCE allele alignments (n=150), (c) STACEY species tree from UCE IUPAC consensus alignments (n=150) and (d) SNAPP species tree from SNP data (1 SNP per locus if present, n=598). Shown are the maximum clade credibility tree (node values = PP, error-bars = 95% HPD of divergence times) and a plot of the complete posterior species tree distribution (excluding burn-in).

which returned the same tree topology (Supplementary Figs. S5 and S6 available on Dryad).

*Species delimitation.*— While the inferred species tree topology is consistent between all four sequence-based MSC analyses (Figs. 6a to 6d), the inferred node heights on the other hand vary greatly between the species trees resulting from the different data processing schemes. For both, the contig sequence data (Fig. 6a) and the chimeric allele data (Fig. 6d), the node heights within the five simulated species (D,E,X,Y,Z) are estimated too high, which leads to an overestimation of the number of coalescent species in the dataset (see similarity matrices). The phased allele data (Fig. 6b) and the IUPAC consensus data (Fig. 6c) on the other hand correctly estimate and delimit the five coalescent species from the simulation input tree (Fig. 6g). The STACEY results show the same pattern in all ten simulation replicates (Supplementary Fig. S7 available on Dryad)

*Accuracy of divergence time estimation.*— For all four sequence-based analyses (Figs. 6a to 6d) the substitution rate was set to '1' for one random locus, and substitution rates for all other loci were estimated relative to this value. Under these settings, we expect the absolute values of the sequence-based analyses to return the node height values of the simulation input tree, which used substitution rates scaled in the same manner. The phased allele MSAs produce the most accurate estimation of divergence times out of all tested datasets (see proximity of estimates to simulation input value, represented by green line in Fig. 7). This is the case for all nodes in the species tree, namely (D,E), (Y,Z), (X,(Y,Z)), and ((D,E)(X,(Y,Z))). While the phased allele data lead to a slight underestimation of divergence times for the very young clades (D,E) and (Y,Z), the heights of the deeper nodes on the other hand are very accurately estimated by these data (Fig. 7). This is in contrast to the contig MSAs and the chimeric allele MSAs, which consistently overestimate the height of all nodes, while the IUPAC consensus MSAs lead to a consistent

underestimation of the height of all nodes (Fig. 7. These biases are present across all simulation replicates while the phased allele data produces the best estimation of divergence times in 88% of the cases (Supplementary Fig. S8 available on Dryad).

### *Additional Analyses*

We ran additional analyses of the contig and the phased allele MSAs for both the empirical and simulated data using a summary coalescent approach as implemented in MP-EST (Yu et al. 2007), which can be found in online Appendix 2 and Supplementary Figs. S9 to S11 (available on Dryad).

## Discussion

### *Allele Phasing is the Preferred Data Processing Scheme*

In this study we tested whether phylogenetic inference improves by phasing sequence capture data into allele sequences, in comparison to the standard workflow of analyzing contig sequences (Faircloth et al. 2012; McCormack et al. 2012; Smith et al. 2014; Faircloth 2015). The answer is yes. We find that phased allele data outperform contig sequences in terms of estimation of divergence times (Fig. 7) and species delimitation (Fig. 6). Contig sequence MSAs lead to a consistent overestimation of divergence times (Fig. 7), which in turn lead to an overestimation of the number of coalescent species in our simulated data (Fig. 6a. This constitutes further support to the finding of Lischer et al. (2014), who conclude that consensus sequences introduce a bias toward older node heights. The phased allele MSAs on the other hand accurately estimate divergence times (Fig. 7) and the number of coalescent species in our simulated data (Fig. 6b).

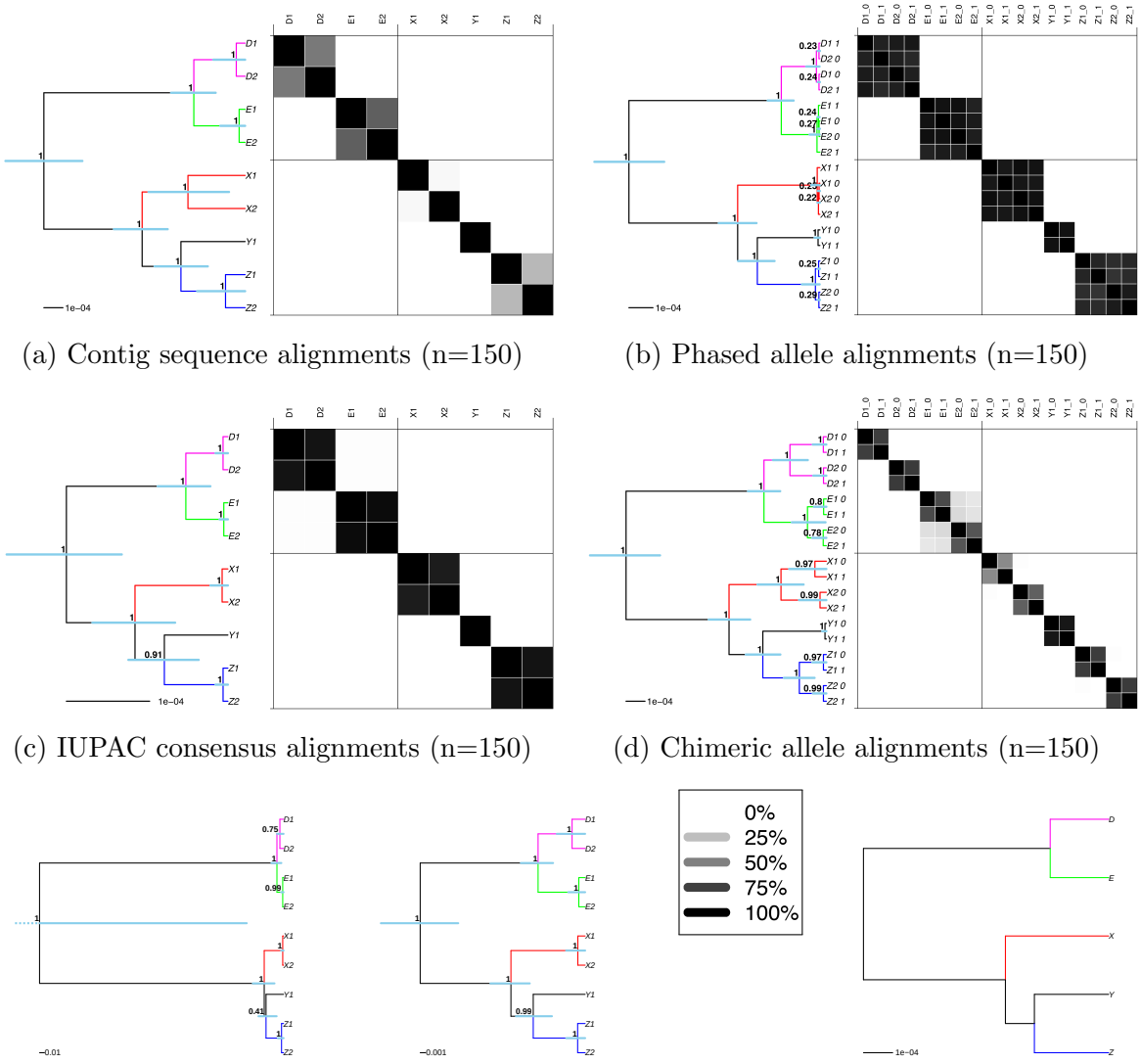


(a) Contig sequence alignments (n=150)

(b) Phased allele alignments (n=150)

(c) IUPAC consensus alignments (n=150)

(d) Chimeric allele alignments (n=150)

(e) SNPs reduced (n=150)

(f) SNPs complete (n=820)

(g) Simulation species tree

Figure 6: MSC species tree results for different data processing schemes of simulated data. (a) to (d) show the STACEY results of the four different types of MSAs analyzed in this study (see sub-figure captions). Displayed in these panels are the maximum clade credibility trees and the similarity matrices depicting the posterior probability of two samples belonging to the same clade, as calculated with SpeciesDelimitationAnalyser. Dark panels depict a high pairwise similarity, while light panels depict low similarity scores (see legend). (e) and (f) show the maximum clade credibility trees resulting from SNAPP for our two SNP datasets, (reduced and complete). (g) shows the species tree under which the sequence data was simulated in this study. Node support values in PP, blue bars representing 95% HPD confidence intervals.

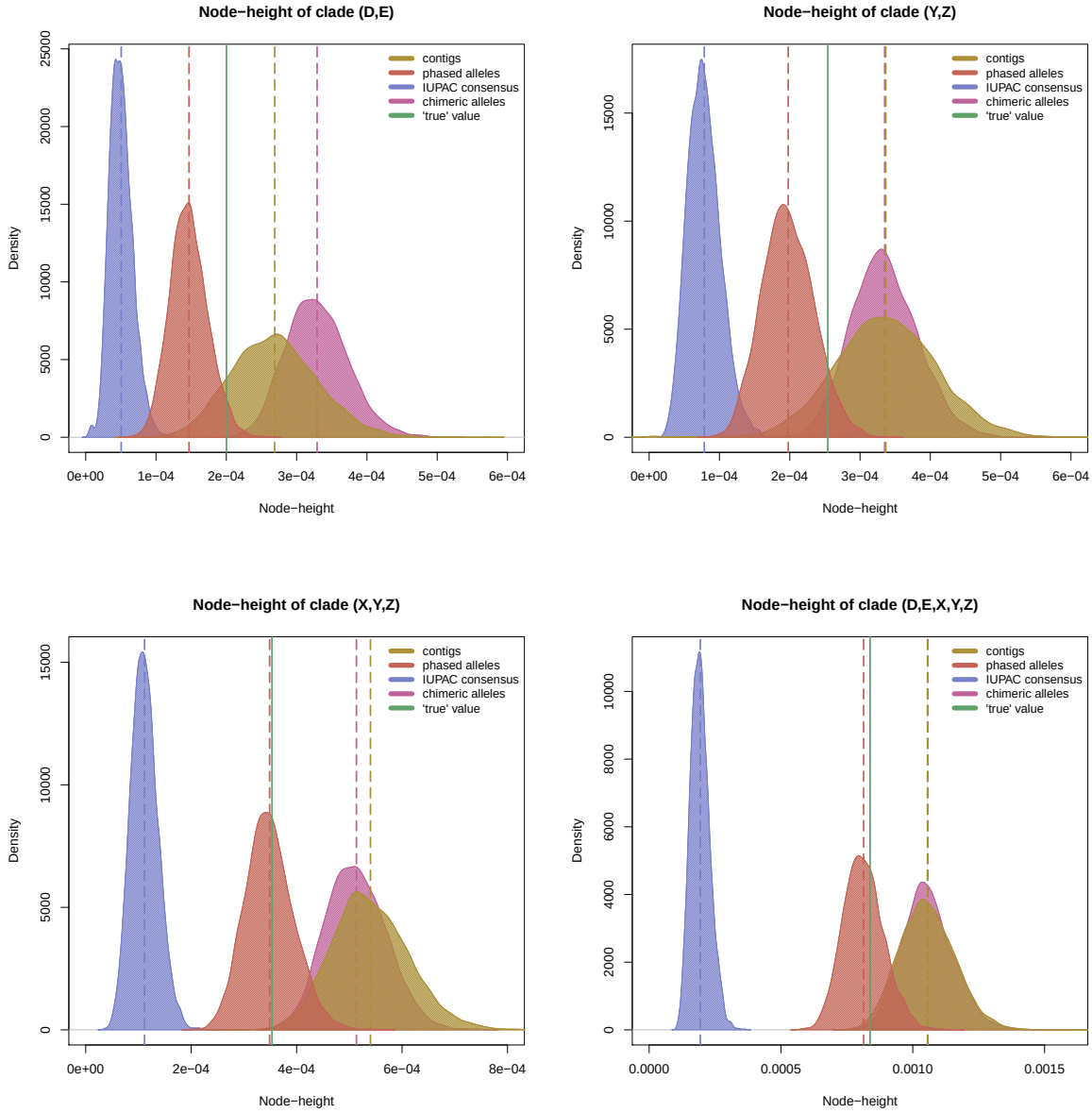


Figure 7: Allele sequences return highest accuracy of node-height estimates. Each sub-figure shows several density plots of node-height estimates for a different node in the STACEY species tree (see sub-figure titles). The four density plots in each sub-figure represent the posterior distribution of node heights (excl. 10% burnin), as estimated by STACEY for the four different data processing schemes tested in this study: contig sequences (yellow), phased allele sequences (red), IUPAC consensus sequences (blue) and chimeric allele sequences (pink). The dotted lines show the means of these posterior distributions. The solid green line shows the 'true' node height value, which is the node height for the respective clade in the input species tree, under which the sequence alignments were simulated.

Besides these qualitative advantages of using phased allele sequences for phylogenetic analyses, there are further theoretical arguments for compiling and analyzing allele sequence MSAs from sequence capture datasets.

First and foremost allele sequences represent the smallest evolutionary unit on which selection and other evolutionary processes act. Therefore the coalescent models that underly our phylogenetic methods, including the MSC model Degnan and Rosenberg (2009), have been developed for allele sequences. Contig sequences on the other hand represent an artificial and possibly chimeric sequence construct which arises from merging all read variation at a given locus into a single sequence. This process masks heterozygous information by eliminating one of the two variants at a heterozygous site (Fig. 4). This shortcoming of the most common assemblers (e.g. ABYSS, Trinity and Velvet) is due to the fact that they were designed to assemble haploid sequences and are not optimized for heterozygous sequences or genomes (Bodily et al. 2015). This makes it obvious why it is preferable to apply allele sequences and not contig sequences for inferring phylogenies.

Second, not only are allele sequences the more appropriate data type but phasing sequence capture data also leads to a doubling of the effective sample size, since two sequences are compiled for a diploid individual, in contrast to only a single sequence per individual in the contig approach. We demonstrate in this study how these sequences can effectively be treated as independent samples from a population by using the assignment-free BirthDeathCollapse model as implemented in STACEY. Since STACEY requires no a priori assignment of sequences to taxa, this avoids a violation of the MSC, which would occur when analyzing allele sequences as separate taxa in the regular *BEAST, since *BEAST assumes each taxon to constitute a separate coalescent species.

Third, sequence capture datasets such as UCEs are perfectly suitable for allele phasing due to their increased read coverage of specific regions which are typically in a suitable size range for read-connectivity based phasing (several hundred to few thousand

base pairs). The workflow developed in this study is now fully integrated into the PHYLUCE pipeline, making allele phasing and SNP extraction for sequence capture data easily available to a broad user group.

Given the mentioned advantages of allele sequences over contig sequences and given the easy availability of the processing workflow, we recommend that allele phasing should become the standard practice for future sequence capture studies.

## *Phasing of Heterozygous Sites Matters*

Several studies have been accounting for heterozygosity by inserting IUPAC ambiguity codes into their sequences at heterozygous sites Potts et al. (2014); Schrempf et al. (2016), rather than phasing heterozygous positions and producing separate allele sequences. Here we directly compare these two approaches and find that the IUPAC consensus sequences perform equally well to the phased allele sequences in terms of species tree topology and species delimitation (Fig. 6). However, the IUPAC consensus sequence data led to a consistent underestimation of the divergence times of all node in the species tree (Fig. 7). This is the opposite pattern found by (Lischer et al. 2014), who reported an overestimation of divergence times for alignments containing IUPAC ambiguity codes. These opposite findings may be caused by the different tree inference programs that were applied between our study and (Lischer et al. 2014). In their study (Lischer et al. 2014) applied a Neighbour Joining (NJ) tree algorithm as implemented in the software PHYLIP Felsenstein (2005), which treats two sequences containing the same ambiguity codes as identical. In effect, (Lischer et al. 2014) did not truly investigate the effect of IUPAC ambiguity codes on phylogenetic estimates but rather the effect of removing heterozygous sites. Our approach of analyzing IUPAC consensus sequences under the MSC in STACEY on the other hand properly integrates these IUPAC ambiguity codes into the calculation of the gene tree likelihoods. Thus we conclude that IUPAC ambiguity codes introduce a bias

toward younger divergence times, even when properly integrating IUPAC ambiguities into the phylogenetic model. COAUTHORS: ANY HYPOTHESES WHY??

We also tested if the better performance of phased allele sequence data may be a mere effect of doubling the number of sequences in the MSAs, since we are producing two allele sequences for each individual rather than one contig sequence. Therefore we generated a dataset of chimeric allele sequences, which contains the same number of sequences as the phased allele data, but all heterozygous positions within an individual are randomly shuffled between the two allele sequences. Just as the contig data, the chimeric allele data led to an overestimation of the number of coalescent species (Fig. 6d) and to a biased estimation toward older divergence times (Fig. 7). The fact that contig sequences and chimeric allele sequences produce very similar results in our analyses is not surprising, since contigs themselves represent chimeric consensus sequences of the variation found at a locus within an individual. However, this result does demonstrate that the number of sequences being analyzed does not affect the phylogenetic estimation in terms of topology, species delimitation and divergence time estimation (Figs. 6 and 7).

Based on these findings we conclude that proper phasing of heterozygous positions is crucial and is clearly preferable to the alternative of coding heterozygous sites as IUPAC ambiguity codes, particularly when the estimation of divergence times is of interest. Further, allele sequences are the theoretically more appropriate input for coalescent models and should thus always be the preferred data type for phylogenetic studies.

## *UCEs as source for SNP data*

Due to the size (number of loci) of many sequence capture datasets, it is often unfeasible to analyze all MSAs jointly in one MSC analysis (Smith et al. 2014; Manthey et al. 2016) due to computational limitations. For all sequence based MSC analyses in this study, we reduced the UCE dataset from 820 loci to 150 loci in order to reach convergence of the

MCMC within a reasonable time frame (three to four days, single core on a Mac Pro, Late 2013, 3.5 GHz 6-Core Intel Xeon E5 processor). However, a viable approach of data reduction while keeping the multilocus information of all loci, is to analyze only a single polymorphic position per MSA using SNAPP Bryant et al. (2012). In our study, this approach produces the correct species tree topology and also estimates the relative node-heights correctly (Fig. 6f). However, SNAPP can only estimate relative and not absolute values for divergence times Bryant et al. (2012), in contrast to the sequence based analyses Figs. 6a to 6d, which deliver absolute divergence time estimates.

Sequence capture datasets such as UCEs provide a suitable data source to extract both, full sequence alignments and SNP datasets of sufficient size for a robust species tree estimation. Even though sequence capture data are not commonly thought about as a source of SNP data, they can in many cases even be preferable to other sequencing techniques, such as RAD sequencing, for producing SNP data. This is because sequence capture data yields a sizable complete SNP matrix (SNPs recovered for all individuals), due to the targeted sequence enrichment prior to sequencing. In our case the complete matrix of unlinked SNPs in the empirical data consisted of 598 positions, which were present and sufficiently supported (>three high-quality reads per haplotype) in all taxa. Particularly when evolutionary distances between individuals are large, RAD sequencing and other restriction site based sequencing techniques are not expected to yield many loci shared between all individuals, while UCE data on the other hand are not sensitive to great evolutionary distances Harvey et al. (2016). In those cases the size of the complete SNP matrix resulting from UCE data can exceed that resulting from RAD sequencing. Additionally, UCE data provide hundreds to thousands of full sequence MSAs as well as the complete mitochondrial genome as a byproduct of the sequence enrichment. The mitochondrial genome provides an excellent marker for estimating absolute divergence times (Fig. 3), based on substitution rates of mitochondrial markers which are known for

birds Lerner et al. (2011) and thus is a valuable phylogenetic data source.

In this study we present and make available a new SNP calling approach for sequence capture data. In contrast to other SNP calling softwares such as GATK (McKenna et al. 2010), which use BAM files as input, our approach uses full sequence MSAs as input (see Fig. 2), in order to identify and extract sites in the alignments that show variation between any user-defined group of sequences. Our SNP calling algorithm can technically be applied to any type of sequence alignments (i.e. allele or contig sequence alignments), even though we recommend to work with SNPs extracted from phased allele alignments, as they represent the true heterozygous information. The user can choose whether or not to allow missing data or ambiguities in the extracted positions, whether to extract them in binary format (as e.g. required by SNAPP) or as nucleotides, and if only one SNP per locus or all SNPs should be extracted. Overall we find that extracting SNPs in this manner (from MSAs) is more efficient and straightforward for sequence capture data than alternative methods such as implemented in GATK. This is mainly because, in our approach, the user does not have to revisit the BAM files of all samples for cumbersome and superfluous re-cleaning and re-filtering of the data, but can instead use the already cleaned and filtered information in the MSAs. Particularly after phasing the FASTQ reads into allele sequences in a previous step, there is no need to go back to the BAM files to extract bi-allelic SNPs. Another advantage of our SNP calling script is that the user can choose a binary SNP output, a feature particularly interesting to users planning downstream analyses with SNAPP. Thus our SNP calling mechanism is an easy, open-source and straightforward tool to derive SNP data from any set of multiple sequence alignments.

## *Phylogenetic relationships in Topaza*

In contrast to previous findings that UCE sequences may be too conserved to resolve phylogenetic questions at shallow taxonomic scales (Giarla and Esselstyn 2015), we find

that UCE sequences are well suited for resolving the intraspecific genetic structure in *Topaza*.

*One or two species?.*— Our results show a separation of two lineages within the genus *Topaza* that is dated at ca. 2.4 Ma in the mitochondrial tree (Fig. 3). These lineages are consistent with the previously described morphospecies *T. pyra* (Gould, 1846) and *T. pella* (Linnaeus, 1758), which are generally accepted in the ornithological community (Hu et al. 2000; del Hoyo et al. 2016a). However, the species status of *T. pyra* has been challenged by some authors (Ornés-Schmitz and Schuchmann 2011; Schuchmann 1999). These authors concluded that *Topaza* is a monotypic genus with *T. pyra* being a subspecies of *T. pella*, which they refer to as *T. pella pyra*. Their findings are based on the analyses of plumage coloration, in which they found an "east-west clinal trend of characters" (Ornés-Schmitz and Schuchmann 2011). In contrast, we do not find such an east-west clinal trend in the genetic data. Instead, *T. pyra* is consistently supported as a separate lineage across all analyses, lending no support for the conspecificity of these two taxa (Figs. 3 and 5).

One aim of this study was to evaluate the genetic structure within these two morphospecies *T. pyra* and *T. pella*. The mitochondrial tree shows two divergent clades within *T. pyra* (Fig. 3), but these clades are not supported by the UCE data (Fig. 5), even though the allele sequence data are picking up a signal that possibly indicates that two such clades are in the process of diversifying (Fig. 5b). For *T. pella* on the other hand, we consistently find the same genetically distinct clades throughout all multilocus MSC analyses (Fig. 5), leading us to distinguish between the following populations that are congruent with previous morphological subspecies descriptions:

*Northern T. pella population: T. pella pella.*— For the mitochondrial tree and all MSC species trees, we find the northern *T. pella* samples 5 and 6 to be sister taxa with high support values (98-100% PP, Figs. 3 and 5). Particularly in the mitochondrial tree (Fig.

3), these two samples appear as close sister taxa, separated by only very short terminal branches. Their close position in the mitochondrial tree shows that, even though geographically far apart, samples 5 and 6 share a relatively recent MRCA in the mitochondrial genealogy, indicating some rather recent gene flow. The sampling locality of sample 5 is within the range of the subspecies *T. pella pella*, which mainly extends across the Guiana shield (Peters 1945; Schuchmann 1999; Hu et al. 2000; Ornés-Schmitz and Schuchmann 2011). Given the sampling location of genetically linked sample 6, which also has been morphologically identified as *T. pella pella* (Table 1), we propose to extend the distribution range of *T. pella pella* from the Guiana shield all the way south to the northern Amazon River bank (see map in Fig. 3).

*Southern T. pella population: T. pella microrhyncha.*— In the same manner as for the northern population *T. pella pella*, we also consistently find the southern *T. pella* samples 8 and 9 to be sister taxa (99-100% PP, Figs. 3 and 5). The sampling locations of these two samples are included in the distribution range of the previously recognized subspecies *T. pella microrhyncha*, extending from the southern bank of the Amazon River as far South as Porto Velho (Brazil) at the Madeira River, close to the border to Bolivia (Peters 1945; Schuchmann 1999; Ornés-Schmitz and Schuchmann 2011). This southernmost boundary of *T. pella microrhyncha* is not accepted by Hu et al. (2000), who instead conclude that this southernmost population belongs to *T. pella pella*. In contrast to the findings by Hu et al., our genetic data clearly support the southernmost sample 9 belonging to the same population as sample 8, which was morphologically identified as *T. pella microrhyncha*. This leads us to propose a distribution range of *T. pella microrhyncha* as shown in Fig. 3, in agreement with the findings by Peters (1945),Schuchmann (1999), and Ornés-Schmitz and Schuchmann (2011).

*Estuary region of Amazon River: T. pella smaragdula.*— Our results show a mixed signal

concerning the phylogenetic placement of sample 7, which was collected from the southern estuary region of the Amazon River and morphologically identified as *T. pella smaragdula*. The sampling locality also falls into the range of the subspecies *T. pella smaragdula* (Peters 1945; Hu et al. 2000; Ornés-Schmitz and Schuchmann 2011), with a distribution including the Amazon River estuary and extending north along the coast to French Guiana. All MSC analyses of the UCE sequence and SNP data place sample 7 with high confidence (97-100% PP) as sister to the southern clade *T. pella microrhyncha* (Fig. 5), whereas in the mitochondrial phylogeny this sample is placed as sister to *T. pella pella* in the North.

The discordance between a gene tree and the species tree in a scenario such as this could be the effect of incomplete lineage sorting, which is most likely if the species or clades in question have diverged rather recently and if population sizes are large. Given that the divergence between *T. pella pella* and *T. pella microrhyncha* appears to be considerably deep based on the multilocus data (crown height of *T. pella*) see Fig. 5) and given that mitochondria are generally considered to have only 25% of the population size of nuclear loci, it is rather unlikely that the position of sample 7 in the mitochondrial tree is a result of incomplete lineage sorting in this case. It seems more likely that the separate position of sample 7 in the mitochondrial tree is a result of introgression of the mitochondrial genome from *T. pella pella* into the gene pool of *T. pella smaragdula*. However, a denser taxon sampling would be necessary to further evaluate the evolutionary history of this particular population. The case of sample 7 highlights that the mitochondrial tree presents a single gene tree phylogeny that only shows one of many genealogies and therefore must not be equaled to a species tree phylogeny. Hence it is important to generate multilocus data for an informed inference of the species tree phylogeny.

*Summarizing biogeographic remarks.*— The presence of genetically similar individuals sampled at great geographic distances (e.g. samples 5 and 6) suggests that *Topaza*

hummingbirds maintain relatively frequent gene flow across vast distances of rainforest habitat. At the same time, we find indicators of phylogenetic structure within species, distinguishing samples that are separated by only a small geographic distance (see e.g. samples 6 and 8). These samples are however separated by the Amazon River, which has been found to constitute a dispersal barrier for various species of birds and many other animals (Remsen and Parker 1983; Clair 2003; Hayes and Sewlal 2004; Moore et al. 2008; Fernandes et al. 2012; Ribas et al. 2012; Thom and Aleixo 2015). Even though some hummingbird species are known to disperse across large distances (Wyman et al. 2004; Russell et al. 1994), the Amazon River and its associated habitats (such as seasonally flooded forests) may be part of a complex network of factors that inhibit gene flow among populations of *Topaza* hummingbirds.

# Supplementary Material

Supplemental Figs. S1-S11, Supplemental Tables S1 and S2, online Appendices 1 and 2 and all scripts, data and setup-files relevant to analyses and figures in the manuscript are available from the Dryad Digital Repository:

# Availability

We integrated all scripts and documentation necessary for phasing and SNP extraction as open-source into the PHYLUCE pipeline (`http://https://github.com/faircloth-lab/phyluce/blob/working/bin/snps/`). All data processing and analyses steps executed on the data are stored in bash-scripts on our project GitHub page at `https://github.com/tobiashofmann88/topaza_uce`. We further provide a documented workflow of processing the raw reads into UCE contig alignments at `https://github.com/tobiashofmann88/UCE-data-management/wiki`.

# Acknowledgments

We wish to thank all those ornithologists who have dedicated their time to collecting samples in Amazonia; museum curators for providing us with samples for this study; Brazilian authorities for issuing the permits needed for this work; our lab engineer Anna Ansebo for laboratory assistance; Alexander Zizka for assistance in creating the sampling and range maps; HBW Alive for providing the *Topaza* illustrations; and colleagues at our labs for discussions and feedback. Computational analyses were performed on the bioinformatics computer cluster Albiorix at the Department of Biological and Environmental Sciences, University of Gothenburg.

# Funding

This work was funded by the Swedish Research Council to A. Antonelli (B0569601) and B. Oxelman (2012-3917); the CNPq (grants 310593/2009-3; 'INCT em Biodiversidade e Uso da Terra da Amazônia' 574008/2008-0; 563236/2010-8; and 471342/2011-4), FAPESPA (ICAAF 023/2011), and NSF-FAPESP (grant 1241066 - Dimensions US-BIOTA-São Paulo: Assembly and evolution of the Amazonian biota and its environment: an integrated approach) to A. Aleixo; the European Research Council under the European Union's Seventh Framework Programme (FP/2007-2013, ERC Grant Agreement n. 331024), the Swedish Foundation for Strategic Research and a Wallenberg Academy Fellowship to A. Antonelli.

*

References

Bodily, P. M., M. Fujimoto, C. Ortega, N. Okuda, J. C. Price, M. J. Clement, and Q. Snell. 2015. Heterozygous genome assembly via binary classification of homologous sequence. BMC Bioinformatics 16:S5.

Bolger, A. M., M. Lohse, and B. Usadel. 2014. Trimmomatic: a flexible trimmer for Illumina sequence data. Bioinformatics 30:2114–20.

Bouckaert, R., J. Heled, D. Kühnert, T. Vaughan, C.-H. Wu, D. Xie, M. A. Suchard, A. Rambaut, and A. J. Drummond. 2014. BEAST 2: a software platform for Bayesian evolutionary analysis. PLoS Computational Biology 10:e1003537.

Bryant, D., R. Bouckaert, J. Felsenstein, N. A. Rosenberg, and A. RoyChoudhury. 2012. Inferring species trees directly from biallelic genetic markers: bypassing gene trees in a full coalescent analysis. Molecular Biology and Evolution 29:1917–32.

Clair, C. C. S. 2003. Comparative permeability of roads, rivers, and meadows to songbirds in Banff national park. Conservation Biology 17:1151–1160.

Degnan, J. H. and N. a. Rosenberg. 2009. Gene tree discordance, phylogenetic inference and the multispecies coalescent. Trends in Ecology and Evolution 24:332–340.

del Hoyo, J., N. Collar, G. Kirwan, and P. Boesman. 2016a. Fiery Topaz (*Topaza pyra*). *in* Handbook of the Birds of the World Alive (J. del Hoyo, A. Elliott, J. Sargatal, D. Christie, and E. de Juana, eds.). Lynx Edicions, Barcelona, Spain.

del Hoyo, J., A. Elliott, J. Sargatal, D. Christie, and E. de Juana. 2016b. Handbook of the Birds of the World Alive. Lynx Edicions, Barcelona, Spain.

Drummond, A. J., M. A. Suchard, D. Xie, and A. Rambaut. 2012. Bayesian phylogenetics with BEAUti and the BEAST 1.7. Molecular Biology and Evolution 29:1969–73.

Edwards, S. V., L. Liu, and D. K. Pearl. 2007. High-resolution species trees without concatenation. Proceedings of the National Academy of Sciences 104:5936–5941.

Faircloth, B. C. 2015. PHYLUCE is a software package for the analysis of conserved genomic loci. Bioinformatics 32:786–788.

Faircloth, B. C., J. E. McCormack, N. G. Crawford, M. G. Harvey, R. T. Brumfield, and T. C. Glenn. 2012. Ultraconserved elements anchor thousands of genetic markers spanning multiple evolutionary timescales. Systematic Biology 61:717–26.

Faircloth, B. C., L. Sorenson, F. Santini, and M. E. Alfaro. 2013. A phylogenomic perspective on the radiation of ray-finned fishes based upon targeted sequencing of ultraconserved elements (UCEs). PLoS ONE 8:e65923.

Felsenstein, J. 2005. Phylip (phylogeny inference package) version 3.6. distributed by the author. dep genome sci univ washington, seattle.

Fernandes, A. M., M. Wink, and A. Aleixo. 2012. Phylogeography of the chestnut-tailed antbird (*Myrmeciza hemimelaena*) clarifies the role of rivers in Amazonian biogeography. Journal of Biogeography 39:1524–1535.

Garrick, R. C., P. Sunnucks, and R. J. Dyer. 2010. Nuclear gene phylogeography using PHASE: dealing with unresolved genotypes, lost alleles, and systematic bias in parameter estimation. BMC Evolutionary Biology 10:118.

Giarla, T. C. and J. A. Esselstyn. 2015. The challenges of resolving a rapid, recent radiation: empirical and simulated phylogenomics of philippine shrews. Systematic Biology 64:727–740.

Gnirke, A., A. Melnikov, J. Maguire, P. Rogov, E. M. LeProust, W. Brockman, T. Fennell, G. Giannoukos, S. Fisher, C. Russ, S. Gabriel, D. B. Jaffe, E. S. Lander, and

812 C. Nusbaum. 2009. Solution hybrid selection with ultra-long oligonucleotides for
813 massively parallel targeted sequencing. Nature Biotechnology 27:182–189.

814 Harvey, M. G., B. T. Smith, T. C. Glenn, B. C. Faircloth, and R. T. Brumfield. 2016.
815 Sequence capture versus restriction site associated DNA sequencing for shallow
816 systematics. Systematic Biology Advance Access syw036.

817 Hayes, F. E. and J. A. N. Sewlal. 2004. The Amazon River as a dispersal barrier to
818 passerine birds: effects of river width, habitat and taxonomy. Journal of Biogeography
819 31:1809–1818.

820 He, D., A. Choi, K. Pipatsrisawat, A. Darwiche, and E. Eskin. 2010. Optimal algorithms
821 for haplotype assembly from whole-genome sequence data. Bioinformatics 26:i183–i190.

822 Hu, D.-S., L. Joseph, and D. J. Agro. 2000. Distribution, variation, and taxonomy of
823 *Topaza* Hummingbirds (Aves: Trochilidae). Ornitologia Neotropical 11:123–142.

824 Iqbal, Z., M. Caccamo, I. Turner, P. Flicek, and G. McVean. 2012. De novo assembly and
825 genotyping of variants using colored de Bruijn graphs. Nature Genetics 44:226–232.

826 Jones, G. 2017. Algorithmic improvements to species delimitation and phylogeny estimation
827 under the multispecies coalescent. Journal of Mathematical Biology 74:447–467.

828 Jones, G., Z. Aydin, and B. Oxelman. 2014. DISSECT: an assignment-free Bayesian
829 discovery method for species delimitation under the multispecies coalescent.
830 Bioinformatics 31:991–998.

831 Katoh, K., G. Asimenos, and H. Toh. 2009. Multiple alignment of DNA sequences with
832 MAFFT. Methods in Molecular Biology 537:39–64.

833 Kolaczkowski, B. and J. W. Thornton. 2004. Performance of maximum parsimony and
834 likelihood phylogenetics when evolution is heterogeneous. Nature 431:980–984.

Kubatko, L. S. and J. H. Degnan. 2007. Inconsistency of Phylogenetic Estimates from Concatenated Data under Coalescence. Systematic Biology 56:17–24.

Lerner, H. R., M. Meyer, H. F. James, M. Hofreiter, and R. C. Fleischer. 2011. Multilocus resolution of phylogeny and timescale in the extant adaptive radiation of Hawaiian honeycreepers. Current Biology 21:1838–1844.

Li, H. and R. Durbin. 2010. Fast and accurate long-read alignment with Burrows-Wheeler transform. Bioinformatics 26:589–595.

Li, H., B. Handsaker, A. Wysoker, T. Fennell, J. Ruan, N. Homer, G. Marth, G. Abecasis, and R. Durbin. 2009. The Sequence Alignment/Map format and SAMtools. Bioinformatics 25:2078–9.

Lischer, H. E., L. Excoffier, and G. Heckel. 2014. Ignoring heterozygous sites biases phylogenomic estimates of divergence times: Implications for the evolutionary history of microtus voles. Molecular Biology and Evolution 31:817–831.

Manthey, J. D., L. C. Campillo, K. J. Burns, and R. G. Moyle. 2016. Comparison of target-capture and restriction-site associated DNA sequencing for phylogenomics: a test in cardinalid tanagers (Aves, Genus: *Piranga*). Systematic Biology Advance Access syw005.

McCormack, J. E., B. C. Faircloth, N. G. Crawford, P. A. Gowaty, R. T. Brumfield, and T. C. Glenn. 2012. Ultraconserved elements are novel phylogenomic markers that resolve placental mammal phylogeny when combined with species-tree analysis. Genome Research 22:746–754.

McGuire, J., C. C. Witt, J. V. Remsen, A. Corl, D. L. Rabosky, D. L. Altshuler, and

R. Dudley. 2014. Molecular phylogenetics and the diversification of hummingbirds. Current Biology 24:910–916.

McKenna, A., M. Hanna, E. Banks, A. Sivachenko, K. Cibulskis, A. Kernytsky, K. Garimella, D. Altshuler, S. Gabriel, M. Daly, and M. A. DePristo. 2010. The Genome Analysis Toolkit: a MapReduce framework for analyzing next-generation DNA sequencing data. Genome research 20:1297–303.

Meiklejohn, K. A., B. C. Faircloth, T. C. Glenn, R. T. Kimball, and E. L. Braun. 2016. Analysis of a rapid evolutionary radiation using ultraconserved elements (UCEs): Evidence for a bias in some multispecies coalescent methods. Systematic Biology Advance Access syw014.

Milne, I., G. Stephen, M. Bayer, P. J. A. Cock, L. Pritchard, L. Cardle, P. D. Shaw, and D. Marshall. 2013. Using Tablet for visual exploration of second-generation sequencing data. Briefings in Bioinformatics 14:193–202.

Mirarab, S., R. Reaz, M. S. Bayzid, T. Zimmermann, M. S. Swenson, and T. Warnow. 2014. ASTRAL: genome-scale coalescent-based species tree estimation. Bioinformatics 30:541–548.

Moore, R. P., W. D. Robinson, I. J. Lovette, and T. R. Robinson. 2008. Experimental evidence for extreme dispersal limitation in tropical forest birds. Ecology Letters 11:960–968.

Mossel, E. and E. Vigoda. 2005. Phylogenetic MCMC algorithms are misleading on mixtures of trees. Science 309:2207–9.

Ornés-Schmitz, A. and K. L. Schuchmann. 2011. Taxonomic review and phylogeny of the

879 hummingbird genus *Topaza* (Gray, 1840) using plumage color spectral information.
880 Ornitologia Neotropical Pages 25–38.

881 Peters, J. L. 1945. Check-list of birds of the world. Volume 5 ed. Harvard Univ. Press,
882 Cambridge, Massachusetts.

883 Potts, A. J., T. A. Hedderson, and G. W. Grimm. 2014. Constructing Phylogenies in the
884 Presence Of Intra-Individual Site Polymorphisms (2ISPs) with a Focus on the Nuclear
885 Ribosomal Cistron. Systematic Biology 63:1–16.

886 Rambaut, A., M. A. Suchard, W. Xie, and A. Drummond. 2013. Tracer v1.6.

887 Rannala, B. and Z. Yang. 2003. Bayes estimation of species divergence times and ancestral
888 population sizes using DNA sequences from multiple loci. Genetics 164:1645–1656.

889 Remsen, J. V. and T. A. Parker. 1983. Contribution of river-created habitats to bird
890 species richness in Amazonia. Biotropica 15:223–231.

891 Ribas, C. C., a. Aleixo, a. C. R. Nogueira, C. Y. Miyaki, and J. Cracraft. 2012. A
892 palaeobiogeographic model for biotic diversification within Amazonia over the past three
893 million years. Proceedings of the Royal Society B: Biological Sciences 279:681–689.

894 Russell, R. W., F. L. Carpenter, M. A. Hixon, and D. C. Paton. 1994. The impact of
895 variation in stopover habitat quality on migrant rufous hummingbirds. Conservation
896 Biology 8:483–490.

897 Schrempf, D., B. Q. Minh, N. De Maio, A. von Haeseler, and C. Kosiol. 2016. Reversible
898 polymorphism-aware phylogenetic models and their application to tree inference. Journal
899 of Theoretical Biology 407:362–370.

Schuchmann, K., G. Kirwan, and P. Boesman. 2016. Crimson Topaz (*Topaza pella*). *in* Handbook of the Birds of the World Alive (J. del Hoyo, A. Elliott, J. Sargatal, D. Christie, and E. de Juana, eds.). Lynx Edicions, Barcelona, Spain.

Schuchmann, K. L. 1999. Family Trochilidae (hummingbirds). Pages 468–680 *in* Handbook of the Birds of the World Alive (J. del Hoyo, A. Elliott, and J. Sargatal, eds.) volume 5 ed. Lynx Edicions, Barcelona, Spain.

Simpson, J. T., K. Wong, S. D. Jackman, J. E. Schein, S. J. M. Jones, and I. Birol. 2009. ABySS: a parallel assembler for short read sequence data. Genome Research 19:1117–23.

Smith, B. T., M. G. Harvey, B. C. Faircloth, T. C. Glenn, and R. T. Brumfield. 2014. Target capture and massively parallel sequencing of ultraconserved elements for comparative studies at shallow evolutionary time scales. Systematic Biology 63:83–95.

Sullivan, B. L., C. L. Wood, M. J. Iliff, R. E. Bonney, D. Fink, and S. Kelling. 2009. eBird: A citizen-based bird observation network in the biological sciences. Biological Conservation 142:2282–2292.

Thom, G. and A. Aleixo. 2015. Cryptic speciation in the white-shouldered antshrike (*Thamnophilus aethiops*, Aves - Thamnophilidae): The tale of a transcontinental radiation across rivers in lowland Amazonia and the northeastern Atlantic Forest. Molecular Phylogenetics and Evolution 82:95–110.

Wyman, S. K., R. K. Jansen, and J. L. Boore. 2004. Automatic annotation of organellar genomes with DOGMA. Bioinformatics 20:3252–5.

Yang, Z. 2015. The BPP program for species tree estimation and species delimitation. Current Zoology 61:854–865.

922 Yu, L., Y.-W. Li, O. a. Ryder, and Y.-P. Zhang. 2007. Analysis of complete mitochondrial
923 genome sequences increases phylogenetic resolution of bears (Ursidae), a mammalian
924 family that experienced rapid speciation. BMC Evolutionary Biology 7:198.